Transp Porous Med (2012) 91:459–478
DOI 10.1007/s11242-011-9854-2

An Experimental Study of CO_2 Exsolution and Relative Permeability Measurements During CO_2 Saturated Water Depressurization

Lin Zuo · Samuel Krevor · Ronald W. Falta · Sally M. Benson

Received: 1 April 2011 / Accepted: 25 August 2011 / Published online: 16 September 2011
© Springer Science+Business Media B.V. 2011

Abstract Dissolution of CO_2 into brine is an important and favorable trapping mechanism for geologic storage of CO_2. There are scenarios, however, where dissolved CO_2 may migrate out of the storage reservoir. Under these conditions, CO_2 will exsolve from solution during depressurization of the brine, leading to the formation of separate phase CO_2. For example, a CO_2 sequestration system with a brine-permeable caprock may be favored to allow for pressure relief in the sequestration reservoir. In this case, CO_2-rich brine may be transported upwards along a pressure gradient caused by CO_2 injection. Here we conduct an experimental study of CO_2 exsolution to observe the behavior of exsolved gas under a wide range of depressurization. Exsolution experiments in highly permeable Berea sandstones and low permeability Mount Simon sandstones are presented. Using X-ray CT scanning, the evolution of gas phase CO_2 and its spatial distribution is observed. In addition, we measure relative permeability for exsolved CO_2 and water in sandstone rocks based on mass balances and continuous observation of the pressure drop across the core from 12.41 to 2.76 MPa. The results show that the minimum CO_2 saturation at which the exsolved CO_2 phase mobilization occurs is from 11.7 to 15.5%. Exsolved CO_2 is distributed uniformly in homogeneous rock samples with no statistical correlation between porosity and CO_2 saturation observed. No gravitational redistribution of exsolved CO_2 was observed after depressurization, even in the high permeability core. Significant differences exist between the exsolved CO_2 and water relative permeabilities, compared to relative permeabilities derived from steady-state drainage relative permeability measurements in the same cores. Specifically, very low CO_2 and water relative permeabilities are measured in the exsolution experiments, even when the CO_2 saturation is as high as 40%. The large relative permeability reduction in both the water and CO_2 phases is hypothesized to result from the presence of disconnected gas bubbles in

L. Zuo (✉) · S. Krevor · S. M. Benson
Department of Energy Resource Engineering, Stanford University, Palo Alto, CA 94305, USA
e-mail: linzuo@stanford.edu

R. W. Falta
Department of Environmental Engineering and Earth Sciences, Clemson University, Clemson, SC 29634, USA

this two-phase flow system. This feature is also thought to be favorable for storage security after CO_2 injection.

Keywords CO_2 exsolution · Relative permeability · CT scanning

1 Introduction

In geologic carbon sequestration, compressed carbon dioxide (CO_2) gas is injected into geological formations at depths where the hydrostatic pressure is above the critical pressure to take advantage of the high density of supercritical CO_2 (e.g., 610 g/l at 12.41 MPa, 50°C). However, even deep in the subsurface, the density of CO_2 is still much less than water or typical brines (∼1100 g/l). This makes the injected CO_2 subject to a strong upward buoyancy force. Many studies have been conducted on CO_2 migration in storage reservoirs, evaluating CO_2 plume development in a two-phase flow systems; the effects of permeability and capillary pressure barriers on CO_2 migration; and strategies to minimize unfavorable CO_2 movement (Hesse et al. 2006; Silin et al. 2008; Riaz et al. 2006; Juanes et al. 2006; Saadatpoor et al. 2010; Benson and Hepple 2005; Benson and Cole 2008; Zhang et al. 2004).

Efforts have also focused on the fate of dissolved CO_2 in the storage reservoir (King and Paterson 2005; Leonenko and Keith 2008; Hassanzadeh et al. 2007; Farajzadeh et al. 2007). In particular, studies have demonstrated that gravitational instability resulting from the slightly higher density of CO_2 saturated brine compared to brine without CO_2 (about 1–2%) will lead to the development of natural convection currents. These convection currents can accelerate plume dissolution and improve storage security. Much less effort has focused on the fate of dissolved CO_2 if it moves upward due to injection-induced pressure gradients between the storage reservoir and the overburden.

Carbon dioxide solubility in water is high and increases approximately linearly with pressure until the supercritical pressure is reached (Fig. 1, Duan and Sun 2003). At 12.41 MPa and 50°C, in pure water, the mole fraction of dissolved CO_2 approaches 2.3% (mass fraction of 5.4%). The high solubility of CO_2 in water is favorable for long-term sequestration since dissolved CO_2 is no longer subject to upward buoyancy forces. As a result, solubility trapping is even more secure than structural trapping. Although estimates of the time needed for complete dissolution vary from 100's to 10,000's years (Riaz and Tchelepi 2008), depending on the permeability, geometry, temperature, and salinity of sequestration sites, in many cases a substantial fraction of injected CO_2 will eventually dissolve in the subsurface. While dissolved CO_2 presents a better storage security, risks of leakage still exist. If CO_2 saturated brine is depressurized, the solubility of CO_2 decreases and CO_2 exsolves from solution, expands and forms a separate phase as the fluid pressure continues dropping. This scenario is most likely to occur by vertical upward movement of CO_2 saturated fluids, triggered by an upward pressure gradient, either from overpressure from injection in deeper formations or from underpressure of ground water due to pumping in a shallower formation. Carbon dioxide saturated water could permeate seals that are impermeable to the CO_2 phase in a two-phase system. To understand the risks associated with CO_2 exsolution, this study seeks to observe the formation of exsolved CO_2 during depressurization and to assess the mobility of the CO_2 and water under these conditions.

There is a large body of knowledge about an analogous occurrence in oil reservoirs: the process of solution gas drive. Gas bubbles exsolve from oil, grow, and accumulate when the reservoir pressure drops below the bubble point during primary depletion. The physical mechanisms of bubble formation (nucleation) and bubble growth in porous media

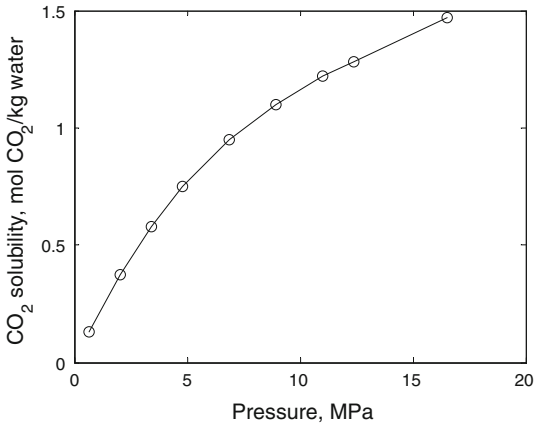

Fig. 1 CO_2 solubility in water at 50°C versus pressure (Duan and Sun 2003)

are well studied in the context of solution gas drive. When pressure decreases, transient gas "nuclei" appear homogenously by thermal fluctuations (Wilt 1989). Firoozabadi and Kashiev (1996) proposed an "instantaneous nucleation" model for a sudden step change decrease in pressure and assume that in a given time the number of bubbles formed only depends on the supersaturation, the porous medium and fluid properties. Then all bubbles grow by diffusion. There is another theory about bubble formation in a porous medium proposed by Yortsos and coworkers (Li and ortsos 1993; Li and Yortsos 1995; Satic et al. 1995). They concluded that the most plausible nucleation mechanism in a porous medium with slow rate of pressure decline is "heterogeneous nucleation," or "progressive nucleation," which postulates various sites on solid surfaces become activated and bubbles arise once the local gas mass concentration is big enough to overcome the local capillary pressure. They also found the final nucleation fraction is a power law of the decline rate. El Yousfi et al. (1997) conducted CO_2–water exsolution experiments in micro models with various pressure drops and concluded that the nucleation is "instantaneous" compared to the long depletion time, but bubbles form only when the pressure drop is big enough to balance the capillary force, which is more similar to "progressive nucleation." Arora and Kovscek (2003) developed mechanistic bubble population balance models with bubble rate equations for both theories. They found both models matched well with experimental data for light and heavy oils. In the progressive nucleation model, the nucleation period was relatively short compared to the total depletion time, which is consistent with the observation of El Yousfi et al. (1997).

Many experiments have been conducted to understand the flow properties of micro bubbles in solution gas drive. An important parameter identified in these experiments is the critical gas saturation. The critical gas saturation is defined as the minimum gas saturation at which evolved micro bubbles start behaving as a separate phase. In other words, the system enters a two-phase flow regime once the gas saturation grows above the critical gas saturation. Before approaching the critical gas saturation, the concept of simultaneous flow of oil and micro bubble gas in solution, referred to as "foamy oil," was first introduced by Smith (1988), but later rejected by experimental observations. Experiments show no gas production until the critical gas saturation is exceeded. After this, the gas flow is intermittent. Reported critical gas saturation values range from 1 to 40% in various experiments (Firoozabadi 2001) and the characteristics of porous media, the properties of fluids and the depletion rate are key causes for the wide spread of reported values. Lower critical gas saturation values are observed with less viscous oils and with slower pressure decline rates (Li and Yortsos 1995). Low

gas relative permeabilities were measured (10^{-6}–10^{-4}) around the critical gas saturation in a system of exsolved gas and oil by Tang and Firoozabadi (2003), and Firoozabadi (2001) further concluded it is the high oil viscosity that contributes to the significant gas mobility reduction.

Although solution gas drive provides a reasonable analogy for CO_2 exsolution, there are significant differences in both fluid properties and the research focus. The high viscosity of oil is thought to be a major factor in solution gas drive mobility reduction. Heavy oil viscosity varies from 10^3 to 10^5 cP while water has viscosity around 0.55 cP at 50°C. The interfacial tension between oil and gas ranges from 0.1 to 5×10^{-5} N/cm, depending on temperature, pressure, and oil composition, but the interfacial tension is an order of magnitude greater for CO_2–water systems (e.g., 33×10^{-5} N/cm for water and CO_2 at 50°C and 12.41 MPa, Georgiadis et al. 2010). Compared with oil/gas, in a CO_2/water system, the work needed to form a spherical nucleus is thus larger and a lower nucleation rate in the CO_2–water system is expected for the same degree of super-saturation compared to the oil–gas system. Once micro bubbles are formed, they are expected to be comparatively more mobile due to the low viscosity of water. Besides these differences in fluid properties, petroleum engineers have a much shorter time horizon of interest than CO_2 storage engineers.

In this study, several CO_2 exsolution experiments are conducted in four distinct rock samples, three Berea sandstones and one Mount Simon sandstone, with X-ray CT scanning. Both rapid and slow depressurizations are applied to achieve CO_2 exsolution from CO_2 saturated water. Exsolved CO_2 and water relative permeability curves in sandstone rocks are measured for the first time. Vertical migration and redistribution of CO_2 micro bubbles were also evaluated after equilibration.

2 Methodology

CO_2 exsolution in a porous media is produced by lowering the pore pressure through the extraction of fluids from a closed volume. Exsolution was first observed by applying rapid pressure drops. Later, a slow depressurization approach was used to measure the critical gas saturation and the exsolved CO_2 and water relative permeabilities in sandstone rocks. After the slow depressurization experiments, the core was sealed to self-equilibrate and the migration and re-distribution of CO_2 during the equilibration was evaluated to support measurements of mobility. The impact of sub-core heterogeneities is also investigated by correlating porosity and CO_2 saturation.

2.1 Experiment and Equipment Description

The experimental setup used for these experiments was designed to conduct steady-state measurements of relative permeability for the CO_2–water system (Perrin and Benson 2010). Modifications were made to accommodate these experiments and are described below. The experimental apparatus is shown in Fig. 2 and consists of the following components: an aluminum core holder surrounded with two electric heaters to maintain the rock sample at a constant temperature during the experiment (50°C is used for these experiments); a confining pressure pump, connected to the core holder to provide a confining pressure outside the rock sample which is kept 2.76 MPa higher than the pore pressure; a two-phase separator with an ultrasonic transducer for fluid–fluid interface measurement; a backpressure pump serving as a reservoir to regulate the pressure of the whole system; two dual-pump systems, one for water and one for CO_2, each including two pumps attached with a set of programmable

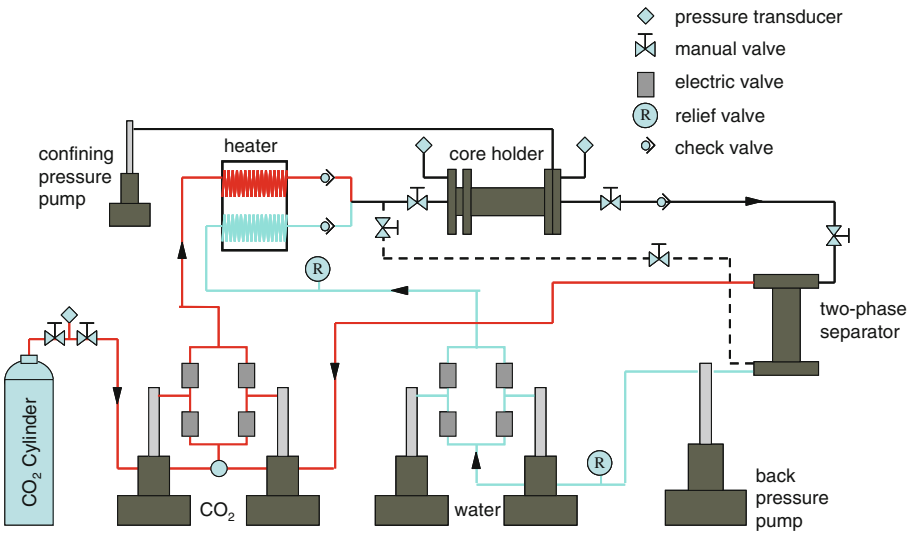

Fig. 2 Experimental Setup for background scans and CO_2 saturated water preparation

electric valves that synchronize pulling of one pump and refilling of the other to maintain a constant flow; and a heater to warm fluids before entering the core holder. Logs of all pumps and the separator are collected automatically. More detailed information about the setup can be found in Perrin and Benson (2010).

Rock samples are 2 inches (~5 cm) in diameter and vary in length, porosity, and permeability (Table 1). Before the experiments, Berea sandstone samples are fired at 700°C to stabilize the clay fraction. The Mount Simon rock sample is not fired to preserve the original flow properties of the rock. Then the core is triple wrapped in (1) heat-shrinkable Teflon sleeve, (2) nickel foil to prevent diffusion of CO_2, and (3) a second Teflon sleeve. A viton rubber sleeve separates the core from the confining fluid used to maintain realistic stresses in the rock (2.75 MPa overpressure for these experiments).

An X-ray CT scanner is used to scan rock samples for measurements of porosity and CO_2 saturation by density difference (Akin and ovscek 2003). 2D images can be taken at a minimum interval of 1 mm along the length of the rock sample and re-constructed as a 3D image. The X-ray scanner is set at a 200 mA current, 120 kV voltage, and 25 cm DFOV protocol. The resolution of each 2D image is 490 × 490 microns per pixel.

2.2 Experiment Methods and Data Processing

By extracting fluids from the water-saturated rock, the pore pressure is reduced from an initial value of 12.41 MPa, resulting in a reduction in CO_2 solubility, triggering the exsolution of CO_2. Two rates of depressurization were used in separate experiments. In one group of experiments, after the water saturated rock sample containing dissolved CO_2 was prepared, a rapid pressure drop was applied to the rock sample, after which time multiple X-ray CT images of the fluid-saturated rock could be made. These experiments were used to investigate the spatial distribution of exsolved CO_2 in the porous media.

In a second set of experiments, a slow depressurization was applied to measure the relative permeability curves of exsolved CO_2 and of water. With this information, comparisons

Table 1 Experiment arrangement

Experiment #	Rock sample characteristics		Depressurization approaches	Intermediate pressure stages
1	Berea sandstone homogeneous	$k = 266$ mD; $\emptyset = 18.7\%$; 9.52 cm in length	Rapid	9.65 MPa, 6.89 MPa, 5.52 MPa
2	Berea sandstone heterogeneous	$k = 439$ mD; $\emptyset = 21.0\%$; 15.24 cm in length	Rapid	6.89 MPa
3	Berea sandstone homogeneous	$k = 963$–1066 mD; $\emptyset = 22.7\%$; 10.16 cm in length	Slow: 0.01, 0.1, 2 ml/min	8.27 MPa, 5.52 MPa
4	Same as #3	Same as #3	Slow: 0.1, 2, 10 ml/min	N/A
5	Mount Simon sandstone homogeneous	$k = 15.7$ mD; $\emptyset = 23.9\%$; 9.04 cm in length	Slow: 0.1, 8 ml/min	N/A

could be made with standard core flooding experiments and solution gas drive experiments performed by other groups. In the experiments, after the initial pressure drop, the core is sealed to observe the evolution of the gravity capillary equilibrium. Also, porosity and CO_2 saturation distributions are compared to study any sub-core scale correlation, since a positive correlation was found in core flooding experiments indicating a strong influence of sub-core scale heterogeneities on flow properties (Perrin and Benson 2010).

Four different rock samples of two rock types are used to understand the influence of rock properties, such as permeability, porosity, and heterogeneity, on the exsolution phenomena. Two homogenous Berea sandstone samples and one heterogeneous Berea sandstone sample with various permeabilities and porosities are used. One Mount Simon sandstone sample with relatively low permeability is also chosen. Capillary pressure curves using a mercury injection porosimeter are obtained before the experiments for prediction of gravity capillary equilibrium and comparisons with experimental observations. Rock samples and different depressurization approaches used are listed in Table 1.

2.2.1 Background X-ray CT Scans and Preparation of CO_2 Saturated Water

An X-ray CT scan of the dry rock core is taken before injecting CO_2 gas to displace air. A series of scans are taken with the core fully saturated with CO_2 at various pressures, covering the range over which the experiments will occur. The core is then depressurized to atmospheric pressure. Next, at least ten pore volumes of fresh water are flowed through the rock sample. The system is then re-pressurized while continuing to flow water so that residual CO_2 is dissolved and all of the pore space is filled with water. The absolute permeability of the rock sample is then determined by measuring the pressure drop across the core over a range of flow rates. A background scan of the core saturated with water is taken when the pore pressure reaches 12.41 MPa. Fluid flow is then stopped and the rock sample is isolated by closing valves at both ends of the core holder.

To prepare CO_2 saturated water at elevated temperatures and pressures, CO_2 and water are circulated together in a loop that bypasses the core. The system is operated continuously for

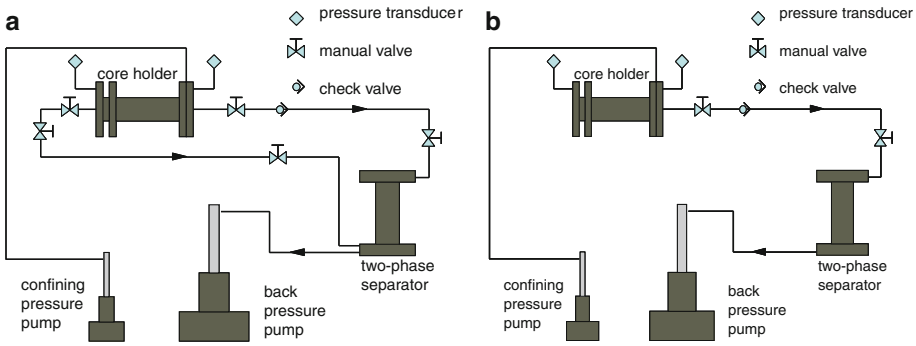

Fig. 3 Experimental Setup for depressurization (**a** rapid depressurization, **b** slow depressurization)

at least 12 h to establish equilibrium between CO_2 and water. Since the fluids are circulated in a closed system, the volume of CO_2 lost due to dissolution can be calculated from a mass balance based on logs of the backpressure pump, water pumps, CO_2 pumps, and the two-phase separator. Demonstration that equilibrium between the fluids is achieved is determined when the volume of separate phase CO_2 in the system stabilizes. Also, any possible leakage can be easily identified if the volume of CO_2 in the system decreases over the experiment.

Once the CO_2 and water are equilibrated, valves isolating the core holder are re-opened and CO_2 saturated water is flooded through the core displacing fresh water. After pumping at least ten pore volumes of CO_2-saturated water through the core, a scan is taken of the rock filled with the CO_2 saturated water. Because the CO_2 saturated water is denser than pure water, about 1% at 5% CO_2 mass fraction (Ohsumi et al. 1992), the average CT numbers observed are around one to two Hounsfield unit larger (i.e., more dense) than the values from the pure water scan and show a 0.6–1.2% bulk density increase. After the scan, the fluid flow is stopped and the rock sample is sealed by closing all of the valves.

2.2.2 Depressurization

During the exsolution experiments the pressure is decreased from 12.41 to 2.76 MPa, while maintaining a constant temperature of 50°C. Gas saturation in the core does not continue increasing after the pressure drops below 2.76 MPa. As a result, 2.76 MPa is chosen as the minimum pressure. In some experiments, the pressure drop is halted at several intermediate pressure stages to allow for equilibration of the distribution of fluids in the core. To depressurize the system, a closed route is formed including the core holder, the backpressure pump and the two-phase separator.

Two different configurations are used. In one configuration, fluids are withdrawn as fast as possible from both ends of the rock sample (rapid depressurization, ~1 MPa/min, Fig. 3a). In a second configuration, fluids are withdrawn from one end of the core holder at a sequence of constant rates (slow depressurization, ~20 kPa/min, Fig. 3b). The sequence of constant rates is applied to keep the rate of pressure drop relatively constant. In both configurations, the confining pressure is maintained in the range of 1.38–2.76 MPa above the pore pressure by manually reducing the pressure in the confining pressure pump. Scans are taken during the depressurization process. Once the pore pressure drops to a desired intermediate pressure, the fluid removal is stopped, the core holder is sealed and multiple CT scans are taken.

2.2.3 Data Collection and Processing

Flow rates, pressures, and fluid volumes in the pumps and the pressures at each end of the core holder are recorded every 3 s. The interface height in the two-phase separator is recorded every 21 s.

The CT scanner creates 2D images with CT values in Hounsfield unit. These CT values are linearly transformed from linear attenuation coefficients which are defined as −1000 for air and 0 for water at standard conditions. As a result, $CT_{\text{water}} = 0$, $CT_{\text{air}} = -1000$. To obtain porosity, since the average grain CT value is unknown, two scans are used: a dry scan, when the rock sample is dry and filled with air, and a water saturated scan, when the rock sample is fully saturated with water at the reservoir conditions. The porosity is calculated:

$$\phi = \frac{CT_{\text{water/rock}} - CT_{\text{air/rock}}}{CT_{\text{water}} - CT_{\text{air}}} \tag{1}$$

To determine CO_2 saturation, three scans are needed: a CO_2 scan, when the rock sample is fully saturated with CO_2 at the reservoir conditions, a solution scan, when the rock sample is fully saturated with the dissolved CO_2–water solution at the reservoir conditions, and an experiment scan, when the rock sample is filled with exsolved CO_2 and water at the same pressure as the CO_2 scan. CO_2 scans are taken at 9.65, 8.27, 6.89, 5.52, and 2.76 MPa. The pixel-scale CO_2 saturation of an experiment scan is calculated:

$$S_{CO_2} = \frac{CT_{\text{solution/rock}} - CT_{\text{exp}}}{CT_{\text{solution/rock}} - CT_{CO_2\text{/rock}}} \tag{2}$$

Core-average CO_2 saturations are calculated using core-average CO_2 CT numbers interpolated from existing CO_2 scans with an exponential fit. Slice-average CO_2 saturations are calculated using slice-average CO_2 CT numbers from existing CO_2 scans. For pixel-scale porosity values and CO_2 saturations, ten individual scans are taken for each scan used in the formulas. Then, each pixel CT number is an average of all ten scans. By doing this, the random error of CT scanning is reduced to ±2% for each calculated pixel value. The random error of slice-average and core-average CO_2 saturations is less than ±0.1%.

2.2.4 Relative Permeability Measurements

Measurements of exsolved CO_2 and water relative permeabilities in sandstone rocks are conducted based on the multiphase modification of Darcy's Law. With fluids withdrawn from one end of the core holder, a simple mathematical formula can be derived for relative permeability calculations (Tang and Firoozabadi 2003). With this method, the fluid properties are assumed to be constant across the rock sample. In the experiments, the average pore pressure is on the order of 1 MPa while the pressure gradient across the core is on the order of 1–10 kPa and variation in fluid properties, such as density, viscosity and interfacial tension due to pressure gradients across the core are small. Another requirement for this calculation is that there is no significant CO_2 saturation gradient across rock sample. The validity of this assumption is demonstrated by observations of the saturation, except in the case of low CO_2 saturation. Given the rock sample dimensions, fluid properties and the absolute permeability, two parameters are needed to calculate relative permeabilities: the flow rate of each phase and the pressure drop across the rock sample. The pressure drop across the core is measured directly by a pressure transducer at each end of the core holder. To measure flow rates, two scans are needed, one at time t_1, one at time t_2. The average water flow rate between t_1 and t_2 is:

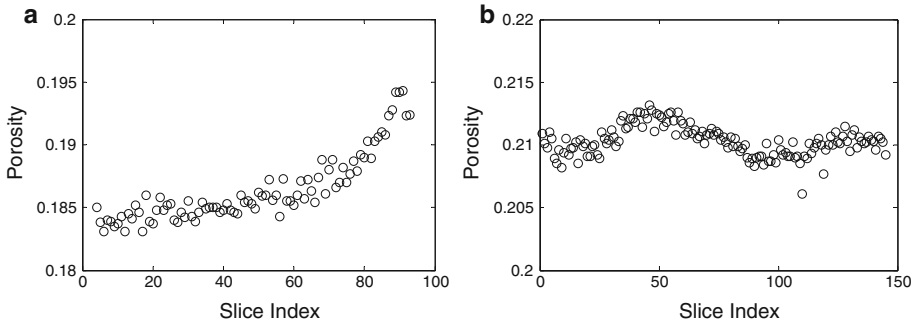

Fig. 4 Slice-averaged porosity for the homogeneous rock sample (**a**) and the heterogeneous rock sample (**b**)

$$q_{\mathrm{w}} = \frac{S_{w1} - S_{w2}}{t_2 - t_1} \cdot V_{\mathrm{p}} \tag{3}$$

and the average CO_2 flow rate between t_1 and t_2 is calculated based on fluids' properties at time t_2:

$$q_{\mathrm{CO_2}} = \frac{S_{\mathrm{CO_2},1} \cdot \rho_{\mathrm{CO_2},1}/\rho_{\mathrm{CO_2},2} + S_{w1} \cdot \Delta/\rho_{\mathrm{CO_2},2} - S_{\mathrm{CO_2},2}}{t_2 - t_1} \cdot V_{\mathrm{p}} \tag{4}$$

where V_{p} is the pore volume and Δ [CO_2 mass/water volume] is the CO_2 solubility change between $p_1(t_1)$ and $p_2(t_2)$. This formula accounts for the expansion of the CO_2 originally in place and additional exsolved CO_2.

To start the measurement, the back pressure pump is set at a low and constant volumetric withdrawal rate. The pore pressure of the rock sample and the pressure drop across the rock sample are recorded every 3 s. At first, the pressure drops very quickly due to the low compressibility of water. Once exsolved CO_2 forms, the withdrawal rate is increased to maintain a relatively constant pressure drop rate (~20 kPa/min).

3 Results

3.1 Evidence for the Development of Exsolved Phase

One homogeneous Berea sandstone and one heterogeneous Berea sandstone (Fig. 4) were used to conduct exsolution experiments using the rapid depressurization approach. The pore pressure was dropped to a specified pressure and then the rock sample was sealed and monitored for 6–24 h to observe equilibration of exsolved CO_2 under the influence of gravity and capillary forces after which the depressurization process started again.

Significant amounts of exsolved CO_2 are observed in these experiments (Fig. 5). The highest CO_2 saturations in both experiments reached over 40% due to solubility reduction and CO_2 expansion as the pressure drops.

CO_2 saturation gradients are observed, especially in the heterogeneous rock sample. Saturation gradients in the homogeneous rock sample are most likely caused by preferential flow out of one end of the core holder rather than equal flow from both ends during the depressurization process. The heterogeneity of rock samples also contributes to the variable CO_2 saturation (Fig. 6). The low porosity portion in the middle of the heterogeneous sample appears to have formed a flow barrier and amplified the flow preference. Compared with

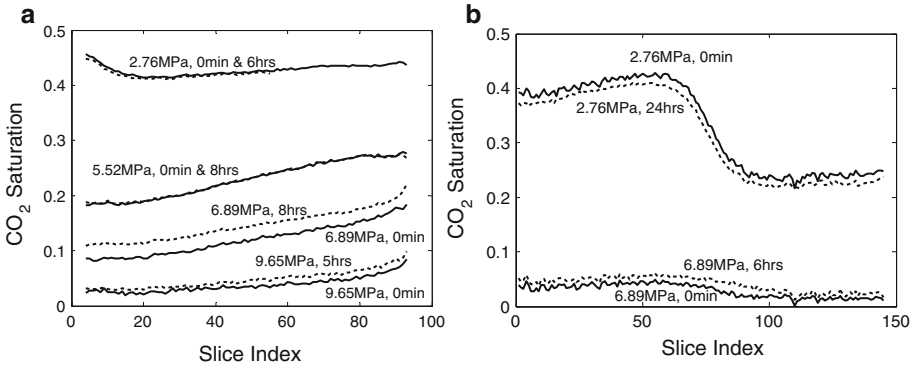

Fig. 5 Slice-averaged CO_2 saturation under various pore pressures and equilibration times for the homogeneous rock sample (**a**) and the heterogeneous rock sample (**b**)

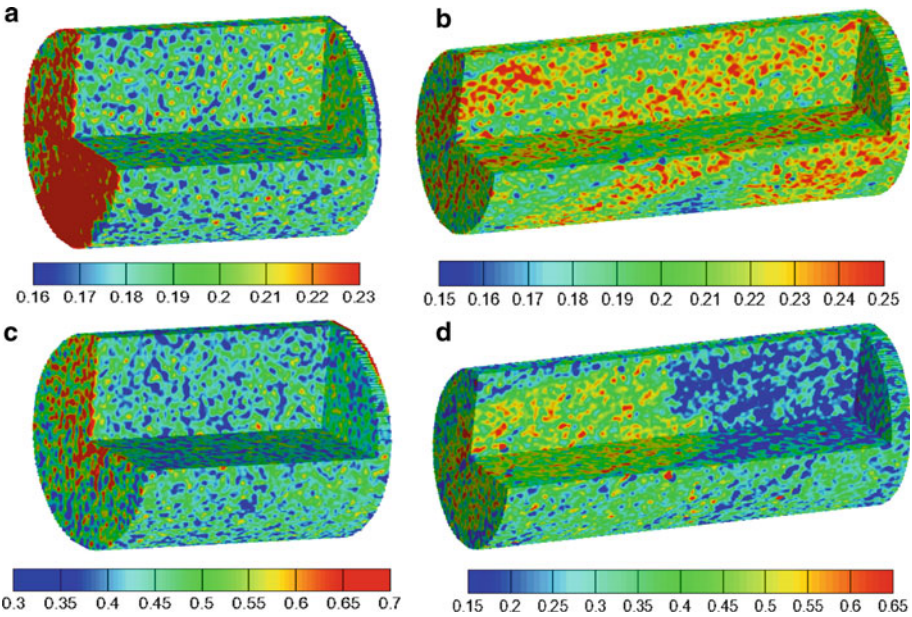

Fig. 6 3D reconstructed porosity and CO_2 saturation images: **a** porosity of the homogeneous rock sample; **b** porosity of the heterogeneous rock sample; **c** CO_2 saturation of the homogeneous rock sample at 2.76 MPa; **d** CO_2 saturation of the heterogeneous rock sample at 2.76 MPa

the results from the homogeneous rock sample which has the same experimental setup, the CO_2 saturation gradients in the heterogeneous rock sample appear to mostly come from the sub-core scale heterogeneities.

3.2 Mobility of Exsolved Phase

The homogeneous Berea sandstone core and a core from the Mount Simon sandstone were used to carry out exsolution experiments with slower depressurization rates. One experiment was conducted in a Berea sandstone with intermediate pressure stages of 8.27 and 5.52 MPa,

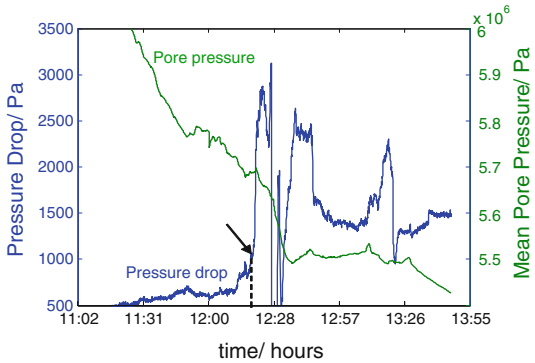

Fig. 7 Mean pore pressure and the pressure drop in experiment #3 around the critical gas saturation. The critical gas saturation was determined by the onset of large pressure drop fluctuation, shown by *arrow*

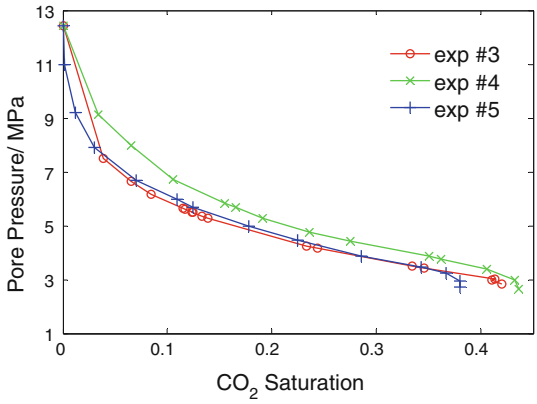

Fig. 8 Pore pressure versus CO_2 saturation during the depressurization

and another experiment was a repetition of the previous one but with a sequence of higher withdraw rates and without intermediate pressure stages. A third experiment was conducted in the much less permeable Mount Simon sandstone without intermediate pressure stages.

3.2.1 Relative Permeability

In experiment #3, the critical point where the gas bubbles become mobile appeared around 12:20, corresponding to a CO_2 saturation of 11.7% (Fig. 7). In the depressurization process, the critical gas saturation is determined from the onset of amplified fluctuations in the pressure drop across the rock sample. In experiment #4 and #5, the critical gas saturations were 15.5 and 11.9%, respectively.

Comparing experiments #3 and #4, it can be seen that the higher withdrawal rates lead to higher gas saturations since water is more mobile and more water is withdrawn out of the core at higher withdrawal rates (Fig. 8). The pressure drop across rock samples (Fig. 9) and flow rates (Figs. 10, 11) are used to compute relative permeabilities in different rock samples (Fig. 12).

During depressurization, the rate of pore pressure decrease slowed as more gas exsolved. The pressure gradient across the samples increased as gas saturation increased until the critical gas saturation was reached. After the critical saturation was reached, the pressure gradient across the sample remained relatively constant. The critical gas saturations corresponding to the turning points in the pressure gradients curves, ∼12%, match well with the

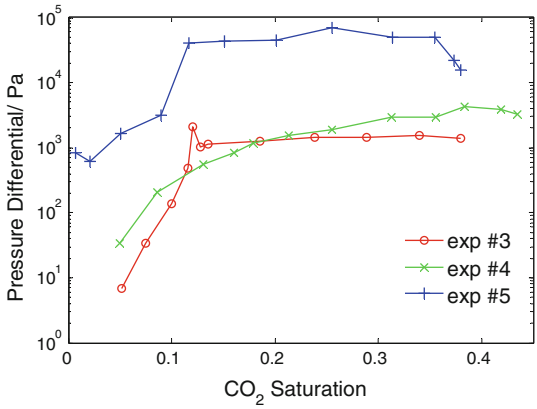

Fig. 9 Pressure drop across the rock sample versus CO_2 saturation during the depressurization

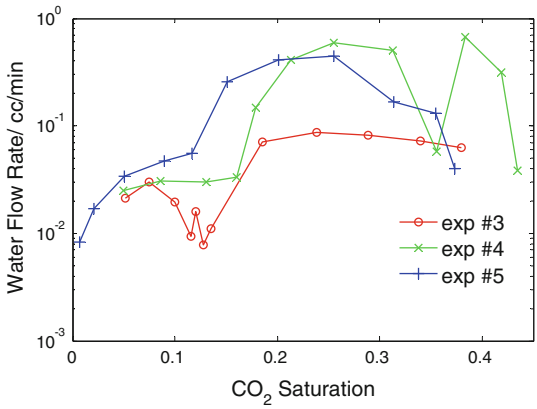

Fig. 10 Water flow rate versus CO_2 saturation during the depressurization

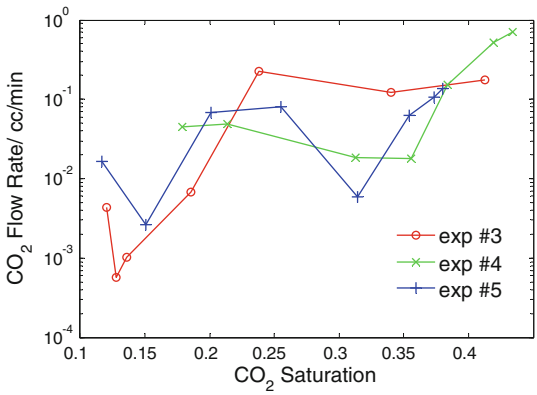

Fig. 11 Exsolved CO_2 flow rate versus CO_2 saturation during the depressurization

transient pressure data, 11.7–15.5%, where when gas bubbles became mobile, as evidenced by the increased amplitude of pressure fluctuations. Flow rates of water and exsolved CO_2 increased as CO_2 saturation grew, but exhibited large fluctuations.

The relative permeability data show very low mobility of both exsolved CO_2 and water. For the exsolved CO_2 phase, the relative permeability is in a range of 10^{-5}–10^{-3} for CO_2

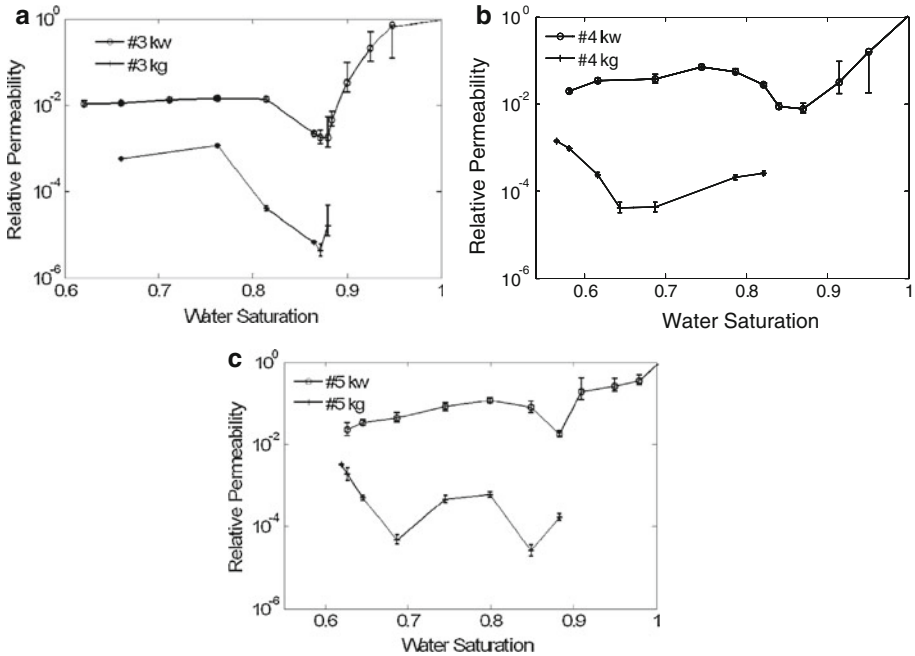

Fig. 12 Exsolved CO_2 and water relative permeability curves in sandstone rocks: **a** experiment #3; **b** experiment #4; **c** experiment #5

saturations of 10–40% (Fig. 12). For the water phase, the relative permeability drops rapidly as CO_2 exsolves, and continues dropping to less than 0.1 as the CO_2 phase becomes mobile.

3.2.2 Porosity, CO_2 Saturation, and Saturation Redistribution

Positive correlations between porosity and CO_2 saturation are often observed in standard core flooding experiments in both homogenous and heterogeneous rock samples at reservoir conditions (Perrin and Benson 2010; Krause et al. 2011). The spatial distribution of CO_2 is shown to be highly influenced by sub-core scale heterogeneity. It is of interest to investigate whether such influence on CO_2 distribution also exists in a system undergoing gas exsolution. If such a correlation does not exist, it further suggests that different factors are controlling the distribution of fluid phases in the rock.

No significant correlation is observed between porosity and CO_2 saturation in experiment #3 immediately after the pore pressure drops to 2.76 MPa (Fig. 13). Therefore, it appears that CO_2 is exsolved from solution uniformly regardless of the variation of porosity. This indicates that sub-core scale heterogeneities and flow processes do not have an important influence on the CO_2 saturation distribution during exsolution of CO_2 from water in a porous media.

After the pore pressure drops to 2.76 MPa, the core holder is sealed and maintained at a constant temperature of 50°C for 260 h for equilibrium. There is a good statistical correlation between CO_2 saturation before and after equilibrium (Fig. 14). The correlation coefficients, r^2, of the regression lines are 0.805, 0.822, and 0.791 for slice #30, #50, and #70, respectively. This indicates little re-distribution of CO_2 is occurring over the 260-h period. The lack

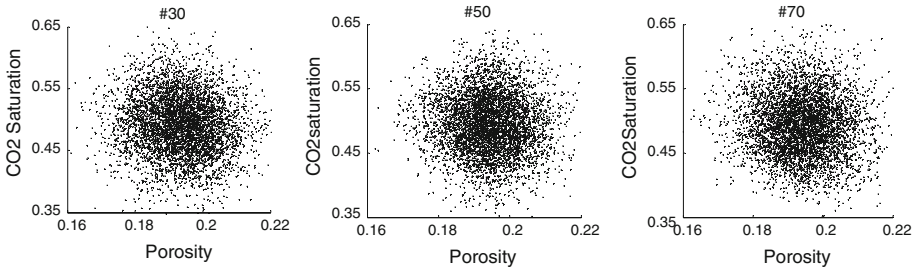

Fig. 13 Scatter plots of porosity and CO_2 saturation at CT slices #30, #50, and #70 in experiment #3. CO_2 saturation was measured immediately after the pore pressure dropped to 2.76 MPa

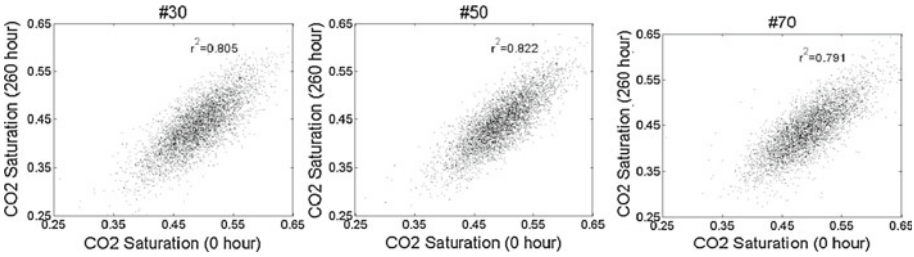

Fig. 14 Scatter plots of the initial CO_2 saturation immediately after depressurization to 2.76 MPa, and the CO_2 saturation measured 260 h after the pore pressure dropped at CT slices #30, #50, and #70 in experiment #3

of fluid re-distribution further supports the very low mobility observed during the relative permeability measurements.

3.2.3 Gravity Effect on CO_2 Saturation Distribution

No vertical CO_2 gradient is observed, even after 260 h of equilibration (Fig. 15). CO_2 saturation at each height is obtained by averaging the center 16 pixels horizontally on the corresponding averaged images. The similarity in CO_2 saturation between 100 and 260 h after depressurization demonstrates that the saturation is changing very slowly, if at all. These curves are compared to the saturation distribution calculated for a homogeneous core allowed to achieve gravity–capillary equilibrium. The calculation is based on the measured capillary pressure curve (Fig. 16) and assumes that the gravity capillary equilibrium is reached:

$$hg\Delta\rho = P_c(S_{max}) - P_c(S_{min}) \tag{5}$$

where h is the height of the rock sample, $\Delta\rho$ is the density difference between water and CO_2 at 2.76 MPa; S_{max} and S_{min} are the top and bottom CO_2 saturation, and a linear distribution is assumed in between.

Under these conditions, if the CO_2 is mobile, a 5% vertical saturation gradient is expected. The lack of a vertical saturation gradient indicates that the CO_2 phase is not sufficiently interconnected and mobile enough to reach gravity capillary equilibrium over the observed time period, despite the high permeability of the core.

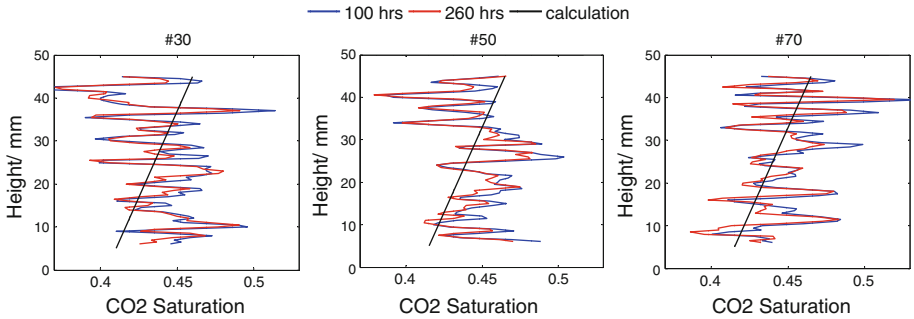

Fig. 15 Vertical CO_2 distribution versus height as equilibrium processed 100 h (*blue curves*) and 260 h (*red curves*) after the pore pressure dropped to 2.76 MPa at CT slices #30, #50, and #70 in experiment #3

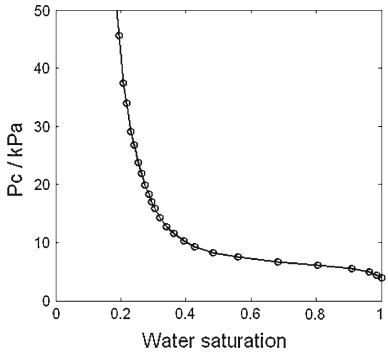

Fig. 16 Capillary pressure curve measured using mercury orosimetry for the homogeneous Berea sandstone used in experiment #3

4 Discussion

4.1 Mobility of Exsolved CO_2

The relative permeabilities from exsolution experiments are compared to relative permeabilities measured using a standard steady-state method on the same cores (Krevor et al. 2011). The exsolved CO_2 relative permeability is far lower than the CO_2 phase relative permeability measured during drainage (Fig. 17). This indicates that in a system undergoing CO_2 exsolution, the use of traditional drainage relative permeability curves to describe the CO_2 phase will lead to large overestimations of the mobility of exsolved CO_2. The significant reduction in both water and CO_2 mobility observed in these experiments could be favorable for storage security after injection. The exsolved gas may form a permeability barrier, preventing further CO_2 migration or even blocking possible leakage paths.

The measured exsolved CO_2 relative permeability is in the same range of that observed in solution gas drive experiments with methane and various heavy oils (Tang and Firoozabadi 2003; Tang et al. 2006). However, the argument that in solution gas drive the viscosity of heavy oil is largely responsible for significant gas mobility reduction is not relevant in the case of CO_2 exsolution, since water is much less viscous than heavy oil and CO_2 and methane have similar viscosities at reservoir conditions.

Instead, it appears that the dispersed morphology of the exsolved CO_2 phase causes the mobility reduction. Under normal two-phase flow conditions during drainage, both the non-wetting phase (CO_2 in this case) and wetting phase are continuous. In addition, CO_2

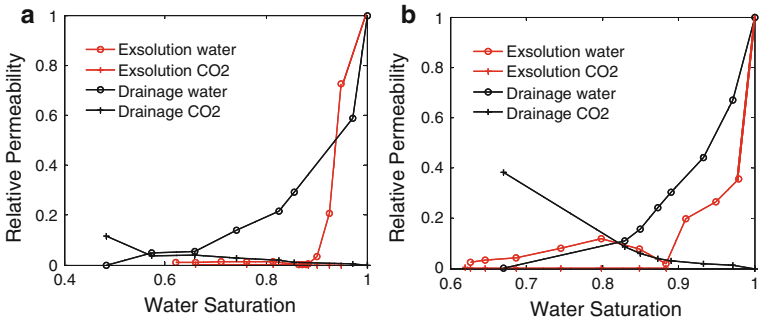

Fig. 17 Comparison between relative permeability curves of xsolved CO_2 and water and standard steady-state core flooding experiments (**a** Berea sandstone; **b** Mount Simon sandstone)

occupies a network of the largest interconnected pores, thus leading to moderate relative permeabilities (Silin et al. 2010). In the case of exsolved CO_2, the non-wetting phase is largely discontinuous, with individual gas bubbles that are poorly aggregated. In part, the low mobility of CO_2 can be attributed to the lack of a continuous phase. In addition, a significant of fraction of the CO_2 is likely to be trapped in the mid to small size pores, where the pressure needed to overcome the capillary forces to move through the pore throats is too large. Even as large exsolved CO_2 phase saturations are achieved, the relative permeability remains low, suggesting that only a small fraction of the exsolved CO_2 forms a continuous phase while most remains disconnected. As a result, the exsolved CO_2 phase may be trapped at saturations much higher than expected from traditional drainage-imbibition multiphase flow theory and exhibits similar immobility as a residual phase caused by imbibition. We hypothesize that is the widely distributed, disconnected gas bubbles, and not the high viscosity of the wetting phase, that is main cause of low gas mobility in this case.

Before the CO_2 bubbles become mobile, the flow resistance to water caused by exsolved CO_2 increases exponentially with CO_2 saturation (Fig. 9). This suggests that a trapped CO_2 phase is occupying the pore spaces and reducing the accessible flow paths for water. Once the critical saturation is reached, the pressure drop no longer increases with CO_2 saturation. This indicates that the increasing volume of CO_2 phase in the pore space does not further block the flow of water. We hypothesize that when the CO_2 phase saturation is low, dispersed bubbles occupy the space close to pore throats and have a significant impact on water flow. Once the critical saturation is reached and bubbles become mobile, pore throats are opened and closed intermittently due to intermittent bubble flow. This explains the pressure drop plateau in Fig. 9 and the gas flow as a discontinuous phase.

4.2 Representativeness and Errors of Measured Relative Permeability

These relative permeability measurements are based on the slow depressurization method, which withdraws fluids from only one end of the core (Tang and Firoozabadi 2003). The calculation is based on a simple mathematical derivation, which assumes constant rock and fluid properties. In these experiments the fluid properties vary by less than 10% (e.g., at pore pressure $\geq$2.76 MPa; pressure drop across the core $\leq$0.2 MPa corresponding to a CO_2 density change $\leq$8.5%, a CO_2 viscosity change $\leq$0.3%). Gas saturation gradients during depressurization are small (e.g., in experiment #5, CO_2 saturation varies from 0.09 to 0.15 at 5.76 MPa and from 0.33 to 0.4 at 2.82 MPa). Given the unique flow geometry of this method

for measuring relative permeability, with no flow at the upstream boundary gradually increasing to 100% flow at the downstream boundary, the question arises as to whether the measurements could be unduly biased by heterogeneities in the core. For these experiments, this is unlikely because all of the relative permeability measurements are made using comparatively homogenous cores (experiments #3, #4, and #5) with no obvious bedding planes or sub-core scale heterogeneity.

Another question regarding the representativeness of these measurements stems from the potential for rock/water/CO_2 reactions to alter the permeability of the rock during the experiments. While the composition of both rocks is dominated by quartz, minor amounts of feldspar, calcite, siderite, and dolomite could dissolve when in contact with CO_2 saturated brine and thus alter the permeability of the rock. Since geochemical reactions are not the focus of this study, the composition of the produced water is not monitored to evaluate the extent of mineral dissolution. However, permeability measurements before and after the experiments demonstrate that the effect of geochemical reactions on permeability is small. The permeability of the Berea core used for two consecutive experiments (#3 and #4) increased from 963 to 1066 mD. The permeability of the Mount Simon core changed from 7 mD (a separate core flooding experiment prior to these experiments) to 15.7 mD prior to exsolution experiment #5. In all cases multiphase flow properties are calculated using the most up-to-date permeability in corresponding experiments to minimize the influence of possible mineral dissolution.

A final issue regarding the low relatively permeabilities observed for both phases is whether they would persist over long time periods and under forced flow conditions. While not an exhaustive study of this issue, we did inject a solution of CO_2-equilibrated water into the Mt. Simon core at the end of the exsolution period and found that the low relative permeability to brine remained unchanged for more than 120 pore volumes, at which point we stopped the experiment. It would be of great interest to further investigate whether the phase mobility measured in flows driven mainly by exsolution and gas expansion is different from pressure gradient driven flows dominated by viscous forces. Not only could the relative permeability be measured under these conditions, but also information about the stability of the exsolved CO_2 could be obtained. If the exsolved CO_2 phase establishes a very stable low relative permeability to water and itself that persist under a forced flow condition, it would be a favorable feature for geological sequestration projects, since once exsolution occurs somewhere, the exsolved gas will increase the flow resistance in that region and hamper further upward flows or even block the flow path. It would be important to study whether such a negative feedback exists in CO_2 exsolution phenomenon.

Flow rates of water and exsolved CO_2 are calculated from mass balances using X-ray CT images with errors less than $\pm 1\%$. The largest errors in these experiments come from the measured pressure drop across the rock. Average pressure drops between scans are used for relative permeability calculations despite the large variations shown in Fig. 6. A relative variation of 20% from the average value is common in pressure drop measurements and 50% in some extreme data points. However, the errors in pressure drop do not have a significant influence on the relative permeability curves as the relative permeability varies over two orders of magnitude while the inaccuracy in pressure drops could only affect the relative permeability by a maximal factor of 2. In general, measurements taken in a lower permeability rock sample with higher withdrawal rates improve the accuracy of the pressure gradient measurements.

5 Conclusions

A series of exsolution experiments have been conducted to understand the phenomenon of CO_2 exsolution associated with depressurization. Conclusions drawn from these experiments are:

1. A significant amount of CO_2 exsolves from solution as pore pressure drops. The CO_2 saturation increases up to 45% as the pressure drops from 12.41 to 2.76 MPa at a constant temperature of 50°C. The experiments demonstrate the possible exsolution scenario and the occurrence of a gas phase as a CO_2 saturated brine moves upward.
2. The critical gas saturation during CO_2 exsolution is recorded as 11.7–15.5%, depending on the depressurization rates and rock types. The recorded critical gas saturation values are within the range summarized by Firoozabadi (2001), 1–40%, from solution gas drive experiments with various oil/gas systems. A higher expansion rate results in a higher critical gas saturation. This is also consistent with observations from solution gas drive studies.
3. CO_2 exsolves uniformly throughout the core and there is no statistical correlation between CO_2 saturation and porosity. This differs greatly from the observations of core flooding experiments co-injecting CO_2 and water, in which a positive correlation was found between saturation and porosity (Perrin and Benson 2010; Krause et al. 2011). The differing observations can be understood from the differing mechanisms (exsolution vs. flow) leading to the presence of CO_2 in the pore space. In the case of exsolution, CO_2 comes out of solution without regard for the pore structure, whereas in multiphase flow, pore structure is the dominant feature determining the distribution of fluids.
4. No vertical re-distribution of CO_2 saturation was observed during equilibration due to the low mobility of gas phase. The expected capillary gravity equilibrium is shown not to develop within 260 h after the initial pressure drop, even in high permeability cores. This also indicates that gas bubbles were not aggregated enough to have sufficient pressure gradients along the vertical dimension of the ganglia to re-distribute.
5. Low water and exsolved CO_2 relative permeabilities are recorded in sandstone rocks. The water relative permeability drops significantly once CO_2 exsolved and remained less than 0.1 after the critical gas saturation is reached. The CO_2 relative permeability is very low, 10^{-5} to 10^{-3}, even when the xsolved CO_2 saturation increases to over 40%. The low CO_2 mobility is consistent with observations from gas solution drive experiments which had reported gas relative permeability of 10^{-4} to 10^{-6} (Tang and Firoozabadi 2003; Tang et al. 2006). The high viscosity of oil is considered the main cause of gas mobility reduction in the gas drive process but it is not the case in CO_2 exsolution as water is much less viscous. Also no comparably large liquid phase mobility reductions have been reported in solution gas drive experiments. The high interfacial tension between water and CO_2 and the discontinuous CO_2 phase are the most significant contributors to the mobility reduction in both the water and CO_2 phases.
6. The significant reduction in both water and CO_2 mobility could be favorable for storage security by preventing CO_2 migration. Studies over much longer time periods than the 260 h reported here need to be carried out to determine if these low mobilities could persist over years to decades.

Acknowledgments This study was funded by the US Environmental Protection Agency, under EPA STAR Grant Number: 834383, and the Global Climate and Energy Project at Stanford. The authors would also like to thank the anonymous reviewers for the many helpful comments about the manuscript.

References

Akin, S., Kovscek, A.R.: Computed tomography in petroleum engineering research. In: Akin, S., Kovscek, A.R. (eds.) Applications of X-ray Computed Tomography in the Geosciences, vol. 215, pp. 23–38. Geological Society, London (2003) (Special Publications, 0305-8719/03/$15. © The Geological Society of London)

Arora, P., Kovscek, A.R.: A mechanistic modeling and experimental study of solution gas drive. Transp. Porous Med. **51**(3), 237–265 (2003). doi:10.1023/A:1022353925107

Benson, S.M., Hepple, R.: Prospects for Early Detection and Options for Remediation of Leakage from CO_2 Equestration Projects. Carbon Dioxide Capture for Storage in Deep Geologic Formations—Results from the CO_2 Capture Project, **2**: Geologic Storage of Carbon Dioxide with Monitoring and Verification. pp. 1189–1203. Elsevier Publishing, Oxford (2005)

Benson, S.M., Cole, D.R.: CO_2 sequestration in deep sedimentary formations. Elements **4**(5), 325–331 (2008)

Duan, Z., Sun, R.: An improved model calculating CO_2 solubility in pure water and aqueous NaCl solutions from 273 to 533 K and from 0 to 2000 bar. Chem. Geol. **193**(3–4), 257–271 (2003)

El Yousfi, A., Zarcone, C., Bories, S.: physical mechanisms for bubble growth during solution gas drive. In: SPE 38921, presented at the SPE Annual Technical Conference and Exhibition, San Antonio, 5–8 Oct 1997

Farajzadeh, R., Salimi, H., Zitha, P.L.J., Bruining, H.: Numerical simulation of density-driven natural convection in porous media with application for CO_2 injection projects. Int. J. Heat Mass Transf. **50**(25–26), 5054–5064 (2007)

Firoozabadi, A., Kashiev, D.: Pressure and volume evolution during gas formation in solution gas drive process. SPE J. **1**(3), 219–228 (1996)

Firoozabadi, A.: Mechanisms of solution gas drive in heavy oil reservoirs. J. Can. Pet. Technol. **40**(3), 15–20 (2001)

Georgiadis, A., Maitland, G., Trusler, J.P.M., Bismarck, A.: Interfacial tension measurements of the (H_2O + CO_2) system at elevated pressures and temperatures. J. Chem. Eng. Data **55**(10), 4168–4175 (2010)

Hassanzadeh, H., Darvish, M.P., Keith, D.W.: Scaling behavior of convective mixing, with application to geological storage of CO_2. AIChE J. **53**(5), 1121–1131 (2007)

Hesse, M.A., Tchelepi, H.A., Orr, F.M. Jr.: Scaling analysis of the migration of CO_2 in saline aquifers. In: SPE 102796, presented at the SPE Annual Technical Conference and Exhibition, San Antonio, 24–27 Sept 2006

Juanes, R., Spiteri, E.J., Orr, F.M. Jr., Blunt, M.J.: Impact of relative permeability hysteresis on geological CO_2 storage. Water Resour. Res. 42:W12418 (2006). doi:10.1029/2005WR004806

King, J.E., Paterson, L.: Role of convective mixing in the long-term storage of carbon dioxide in deep saline formations. SPE J **10**(3), 349–356 (2005)

Krause, M., Perrin, J.C., Benson, S. M.: Modeling permeability distributions in a sandstone core for history matching coreflood experiments. SPE J. (2011, in press)

Krevor, S.C.M., Pini, R., Zuo, L., Benson, S.M.: Multiphase flow properties of CO_2 and water in sandstone rocks at reservoir conditions. Water Resour. Res. (2011, in press)

Leonenko, Y., Keith, D.W.: Reservoir engineering to accelerate the dissolution of CO_2 stored in aquifers. Environ. Sci. Technol. **42**(8), 2742–2747 (2008)

Li, X., Yortsos, Y.C.: Critical gas saturation: modeling and sensitivity studies. In: SPE 26662, presented at the SPE Annual Technical Conference and Exhibition, Houston, 3–6 Oct 1993

Li, X., Yortsos, Y.C.: Theory of multiple bubble growth in porous media by solute diffusion. Chem. Eng. Sci. **50**(8), 1247–1271 (1995)

Ohsumi, T., Nakashiki, N., Shitashima, K., Hirama, K.: Density change of water due to dissolution of carbon dioxide and near-field behavior of CO_2 from a source on deep-sea floor. Energy Convers. Manag. **33**(5–8), 685–690 (1992)

Perrin, J.C., Benson, S.M.: An experimental study on the influence of sub-core scale heterogeneities on CO_2 distribution in reservoir rocks. Transp. Porous Med. **82**(1), 93–109 (2010). doi:10.1007/s11242-009-9426-x

Riaz, A., Hesse, M.A., Tchelepi, H.A., Orr, F.M. Jr.: Onset of convection in a gravitationally unstable diffusive boundary layer in porous media. J. Fluid Mech. **548**, 87–111 (2006)

Riaz, A., Tchelepi, H.A.: Dynamics of vertical displacement in porous media associated with CO_2 sequestration. SPE J. **13**(3), 305–313 (2008)

Saadatpoor, E., Bryant, S.L., Sepehrnoori, K.: New trapping mechanism in carbon sequestration. Transp. Porous Med. **82**(1), 3–17 (2010). doi:10.1007/s11242-009-9446-6

Satic, C., Li, X., Yortsos, Y.C.: Scaling of single-bubble growth in a porous medium. Phys. Rev. E **51**(4), 3286–3295 (1995)

Silin, D., Patzek, T. W., Benson, S. M.: A One-dimensional model of vertical gas plume migration through a heterogeneous porous medium. Int. J. Greenh. Gas Control. ISSN 1750-5836. (2008). doi:10.1016/j.ijggc.2008.09.003

Silin, D., Tomutsa, L., Benson, S. M., Patzek, T. W.: Microtomography and pore-scale modeling of two-phase fluid distribution. Transp. Porous Med. **86**(2), 495–515 (2010). doi:10.1007/s11242-010-9636-2

Smith, G.E.: Fluid flow and sand production in heavy oil reservoirs under solution gas drive. SPE Prod. Eng. **3**(2), 169–180 (1988)

Tang, G.Q., Firoozabadi, A.: Gas- and liquid-phase relative permeabilities for cold production from heavy oil reservoir. SPE Reserv. Eval. Eng. **6**(2), 70–80 (2003)

Tang, G.Q., Sahni, A., Gadelle, F., Kumar, M., Kovscek, A.R.: Heavy-oil solution gas drive in consolidated and unconsolidated rock. SPE J. **11**(2), 259–268 (2006)

Wilt, P.M.: Nucleation rates and bubble stability in water carbon dioxide solutions. J. Colloid Interface Sci. **112**, 530–538 (1989)

Zhang, Y.Q., Oldenburg, C.M., Benson, S.M.: Vadose zone remediation of carbon dioxide leakage from geologic carbon dioxide sequestration sites. Vadose Zone J. **3**, 858–866 (2004)